

Effect of the turbulence modeling in large-eddy simulations of nonpremixed flames undergoing extinction and reignition

Esteban D. Gonzalez-Juez ^{*} and Adhiraj Dasgupta [†]

Combustion Science & Engineering, Inc., Columbia, MD

Salman Arshad [‡] and Michael Oevermann [§]

Chalmers University of Technology, Gothenburg, Sweden

David Lignell [¶]

Brigham Young University, Provo, UT

Simulating practical combustion systems requires the approximation of the interaction between turbulence, molecular transport and chemical reactions. Turbulent combustion models are used for this purpose, but their behavior is difficult to anticipate based on their mathematical formulations, making the use of numerical experimentation necessary. Therefore, the present work explores the effect of three turbulent-combustion models, two eddy-viscosity models, and their parameters on a combustion problem which is notoriously difficult to model: flame extinction and reignition. For this purpose, two types of temporal jets are considered, and direct-numerical-simulation results are compared qualitatively with those from large-eddy simulations.

I. Introduction

Combustion devices such as piston engines, gas-turbine engines, afterburners, and furnaces operate in a turbulent-combustion mode, as opposed to laminar combustion.^{1,2} Turbulent combustion involves an interaction between chemical reactions, micromixing (molecular mixing), and turbulence that spans a broad range in spatiotemporal space. As a result, the full resolution of these physics with Direct Numerical Simulations (DNS) is currently computationally affordable only for the simplest type of problems. Practical problems need to be simulated with mathematical formulations that approximate the above physics. These formulations are called turbulent-combustion models. Being models themselves, careful comparisons of their predictions with experiments or DNS is necessary, a topic which has a vast literature.²⁻⁵ Nonetheless, there still remains various physics which have proven to be particularly difficult to model.

The onset of flame blowout is a dangerous operating condition. It involves extinction and reignition,⁶ both of which pose a difficult modeling challenge. To start with, convenient modeling assumptions about the rate controlling mechanism (mixing-controlled or reaction-controlled) no longer apply. Another difficulty is the fact that some reignition mechanisms involve a distributed-reaction-like regime^{7,8} or a partially-premixed combustion mode.^{9,10} Therefore, for example, flamelet or conditional-moment-closure models designed exclusively for either premixed or nonpremixed combustion are not applicable, but may need to be modified to account for partially-premixed combustion, a task that has been conducted for flamelets.¹¹ Another challenge in modeling extinction and reignition is that molecular diffusion plays a key role; not surprisingly, simulations of extinction and reignition with transported PDF (TPDF) methods, where micromixing is modeled, not resolved, are very sensitive to the type of micromixing model.¹² This type of model-parameter sensitivity is not restricted to TPDF. Moreover, some flames undergoing extinction and reignition exhibit PDFs of temperature with two peaks (i.e. not monomodal PDFs),^{13,14} a feature that cannot be captured

^{*}Senior Engineer, esteban@fastmail.us, AIAA Member.

[†]Senior Engineer.

[‡]Graduate Student.

[§]Professor.

[¶]Professor.

with models assuming PDFs as a sum of two or three delta functions, as done by the multi-environment PDF method as currently formulated. Further discussion of these challenges for turbulent-combustion models is provided elsewhere.^{15–19}

Considering that extinction-reignition problems pose a difficult modeling challenge, the present work uses two reacting temporal jets to assess the predictive capabilities of Large Eddy Simulations (LES). This assessment is conducted by taking the point of view of a user by following the next guidelines. First, predictions from three types of models are compared: the Linear Eddy Model (LEM) turbulent-combustion model;^{20–23} the Partially Stirred Reactor model (PaSR) from Chalmers University of Technology,²⁴ which can be seen as a variant of the ubiquitous Eddy Dissipation Concept (EDC) model;²⁵ and, the no-model or laminar-chemistry or quasi-laminar-chemistry approach. Second, simulations are conducted for two mesh sizes, ranging from those used in academic LES, to those use in industry. Using different mesh sizes is necessary to address the following question: Is the mesh spacing so fine that the use of a turbulent-combustion model is not needed at all? Third, the empirical constants of the turbulent-combustion models are varied. In order to achieve the present objective along these lines, the jets of Hawkes et al.²⁶ and Lignell et al.⁹ are adequate choices because they exhibit extinction-reignition, they have well defined boundary conditions, and they can be simulated with computationally affordable LES, simplifying the conduction of a parametric study. Their drawback, however, is their rather low turbulence levels. In this way, the following seeks a primarily qualitative comparison between DNS and LES results through the use of temperature maps.

II. Approach

II.A. LES equations

The present work uses the OpenFOAM[®] library^{27,28} (v. 2.3.1) and considers the following filtered or averaged conservation equations for mass, momentum, total sensible enthalpy, and species for gases that are compressible, viscous, heat-conducting and multiple-component and move at low-Mach-number speeds:

$$\frac{\partial \bar{\rho}}{\partial t} + \frac{\partial(\bar{\rho} \tilde{u}_i)}{\partial x_i} = 0, \quad (1)$$

$$\frac{\partial \bar{\rho} \tilde{u}_i}{\partial t} + \frac{\partial(\bar{\rho} \tilde{u}_j \tilde{u}_i)}{\partial x_j} = -\frac{\partial \bar{p}}{\partial x_i} + \frac{\partial}{\partial x_j} (\bar{\tau}_{ji} + \tau_{ji}^{sgs}), \quad (2)$$

$$\frac{\partial \bar{\rho} \tilde{h}}{\partial t} + \frac{\partial(\bar{\rho} \tilde{u}_j \tilde{h})}{\partial x_j} = -\frac{\partial}{\partial x_j} (\bar{q}_j + q_j^{sgs}) + \frac{\partial \bar{p}}{\partial t} + \bar{S}_h, \quad (3)$$

$$\frac{\partial \bar{\rho} \tilde{Y}_\alpha}{\partial t} + \frac{\partial(\bar{\rho} \tilde{u}_j \tilde{Y}_\alpha)}{\partial x_j} = -\frac{\partial}{\partial x_j} (\bar{j}_{\alpha,j} + j_{\alpha,j}^{sgs}) + \bar{S}_\alpha. \quad (4)$$

Here ρ is density, p pressure, u_i is the velocity vector, h is the sensible enthalpy, and Y_α is the mass fraction of the species α . The bar denotes a spatial average and the tilde a Favre spatial average. $\bar{\tau}_{ji}$, \bar{q}_j , and $\bar{j}_{\alpha,j}$ are respectively the averaged viscous stress tensor, heat flux, and Fickian molecular flux of species α . Likewise, τ_{ji}^{sgs} , q_j^{sgs} , and $j_{\alpha,j}^{sgs}$ are the subgrid viscous stress tensor, heat flux, and molecular flux of species α , all of which need closure. These conservation equations are complemented with the averaged equation of state for ideal gases,

$$\bar{p} = \bar{\rho} R_u \sum_{\alpha=1}^N \frac{\tilde{Y}_\alpha \tilde{T}}{MW_\alpha}, \quad (5)$$

and the averaged caloric equation of state given by NASA polynomials,

$$\tilde{h}_s = \tilde{h}_s(\tilde{T}). \quad (6)$$

Closure of τ_{ji}^{sgs} , q_j^{sgs} , and $j_{\alpha,j}^{sgs}$ is done mainly with the Smagorinsky model and turbulent Prandtl and Schmidt numbers equal to one. In addition, a low-Reynolds number one-equation-eddy model is used to close these terms. These eddy-viscosity models are used as implemented in OpenFOAM. The averaged source terms \bar{S}_h and \bar{S}_α are closed as follows.

II.B. Closure of the chemical source terms with PaSR and the no-model approach

With the PaSR model in OpenFOAM the averaged chemical source term, \bar{S}_α , is computed with

$$\bar{S}_\alpha = \left(\frac{\tau_c}{\tau_c + \tau_m} \right) \left(\frac{C_\alpha^* - \bar{C}_\alpha}{\Delta t} \right) MW_\alpha, \quad (7)$$

where $\bar{C}_\alpha = \bar{\rho} \tilde{Y}_\alpha / MW_\alpha$, τ_c is a chemical characteristic time defined to be proportional to an average of the forward reaction rate of all reactions and all species. τ_m is the mixing characteristic time given by:

$$\tau_m = c_m \sqrt{\frac{\bar{\mu} + \mu^{sgs}}{\bar{\rho} \epsilon^{sgs}}}, \quad (8)$$

with c_m being a model constant equal to ten unless said otherwise, μ^{sgs} a subgrid-scale eddy viscosity, and ϵ^{sgs} a subgrid-scale dissipation. An important feature of the PaSR model is the computation of C_α^* , which represents the concentration of the specie α at the subgrid level. C_α^* is computed from the solution of the governing equations of a constant-pressure reactor.¹ For this solution, \bar{C}_α and \tilde{T} are used as initial conditions, and the simulation is time-advance from t to $t + \Delta t$ at time intervals of the order of τ_c . Further details about the PaSR model are given elsewhere.²⁴ In the no-model approach, the averaged chemical source term is given by:

$$\bar{S}_\alpha = S_\alpha(\bar{C}_\alpha, \tilde{T}). \quad (9)$$

In other words, the chemical source term is simply evaluated using the resolved fields.

II.C. LEM modeling “inside” a LES cell

The LESLEM model is composed of the following elements: the LES equations discussed above; the LEM modeling “inside” a LES cell discussed right away; the transfer of information from the LEM to the LES; the LEM modeling “between” LES cells; and for the present particular implementation the closure of \bar{S}_h and \bar{S}_α .

The hallmark feature of LEM is a 1D domain consisting of an array or stack of wafers,²³ with an inflow at one end, and an outflow at the other end. There is one array per computational LES cell, as pictured in Fig. 1. The subgrid flow is governed by, among others, the conservation equations in their 1D form:

$$\int \rho \Delta x = m_{cell} \quad (10)$$

$$\frac{\partial T}{\partial t} = -\frac{\partial q_x}{\partial x} + S_T. \quad (11)$$

$$\frac{\partial Y_\alpha}{\partial t} = -\frac{\partial j_{\alpha,x}}{\partial x} + S_\alpha. \quad (12)$$

Here m_{cell} is the total mass in a LES cell, the integration is done over the whole 1D domain, the x coordinate is parallel to the 1D array, and S_T is the heat-source term in the temperature equation. Here unity Prandtl and Lewis numbers are used to compute q_x and $j_{\alpha,x}$.

Macromixing (subgrid turbulent stirring) is represented by distorting the profiles of various quantities according to

$$T(x) \rightarrow T(M(x)), \quad Y_\alpha(x) \rightarrow Y_\alpha(M(x)). \quad (13)$$

Here $M(x)$ is a mapping operation called the triplet map. The effect of the triplet map on a flow property profile defined in $[x_0, x_0 + l]$ is to replace the profile with three compressed images of the original with the middle image flipped. This is how the compressive and rotational motions observed in turbulent flows are represented in LEM.²⁹

Triplet maps are parametrized by a location x_0 , length l , and an eddy rate distribution λ . They are implemented in a stochastic way by sampling x_0 from a uniform distribution and l from

$$f(l) = \frac{5}{3} \frac{l^{-8/3}}{l_p^{-5/3} - l_{max}^{-5/3}}, \quad (14)$$

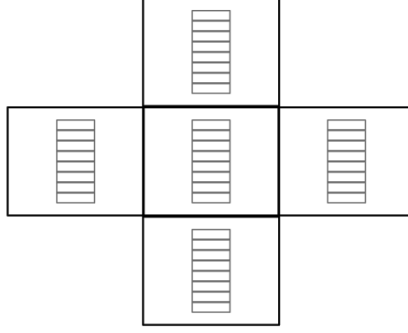


Figure 1. LEM simulations use a 1D domain (grey line) consisting of a stack of wafers (LEM elements) per computational LES cell (black line).

where l_p and l_{max} are the most-probable and maximum length-scales characterizing the turbulence, and are specified by the user. Here l_p is taken as the Kolmogorov length-scale η and l_{max} equals the local mesh spacing of the LES solver Δ . Implied here are Kolmogorov’s scalings in the inertial subrange (e.g. the time-scale of an eddy τ scales as $\tau \sim l^{2/3}$). An estimate for the Kolmogorov length-scale is given by

$$\eta = N_\eta \frac{\Delta}{Re_\Delta^{3/4}}, \quad (15)$$

with N_η being a model constant, and Re_Δ the subgrid Reynolds number:

$$Re_\Delta = \frac{u_{sgs} \Delta}{\nu}, \quad (16)$$

where u_{sgs} is a characteristic subgrid velocity fluctuation, and ν is the kinematic viscosity.

The eddy rate distribution λ is obtained through dimensional reasoning and is computed with

$$\lambda = \frac{54 \nu Re_\Delta \left(\frac{\Delta}{\eta}\right)^{5/3} - 1}{5 C_\lambda \Delta^3 \left(1 - \left(\frac{\eta}{\Delta}\right)^{4/3}\right)}, \quad (17)$$

with C_λ being a model constant. The average time interval between triplet maps is:

$$\Delta t_{stir} = \frac{1}{\lambda \Delta}. \quad (18)$$

Unless said otherwise $C_\lambda = 1$ and $N_\eta = 1.1$ are used throughout. These values were selected to ensure that triplet maps are being implemented during the simulation.

II.D. LEM modeling “between” LES cells

The last element of LESLEM is an algorithm that transfers subgrid-scale quantities, i.e. those defined in the 1D arrays but not necessarily at the LES level, between 1D arrays in adjacent LES computational cells. It is through this algorithm that the 1D arrays “see” the resolved flow in the form of boundary conditions for Eqs. 10-12. Of the various algorithms proposed, the present work uses the splicing algorithm since it has proven to be robust for practical combustion implementations. Basically, the splicing algorithm cuts and pastes the end portions of 1D arrays of adjacent LES cells to emulate a Lagrangian type of mass transfer. Decisions of how much to cut and paste are based on the values of the mass fluxes across the faces of LES computational cells. For example, if the mass flux at a given face of cell A is large and directed from cell A to cell B, a large portion of the 1D array in A will be cut and then pasted onto one of the two endpoints of the array in B. There is some arbitrariness, however, in how this is exactly done. If this mass flux were small, a small portion would be cut and pasted. Details about the splicing algorithm used here are given in App. V.

II.E. Closure of the chemical source terms with LEM

Figure 2 summarizes the steps of the present LEM model to close the chemical source terms. In Fig. 2 μ_{sgs} is a subgrid eddy viscosity, Δ is the filter width or the cell spacing, and Δt is the time step of the LES. The averaged chemical source terms \bar{S}_h and \bar{S}_α is conducted by taking the median value along the various LEM elements for the current LES time step. This calculation is seen to produce almost identical results when using a mean. It is important to note that this use of LEM differs from its more typical one.^{22,23}

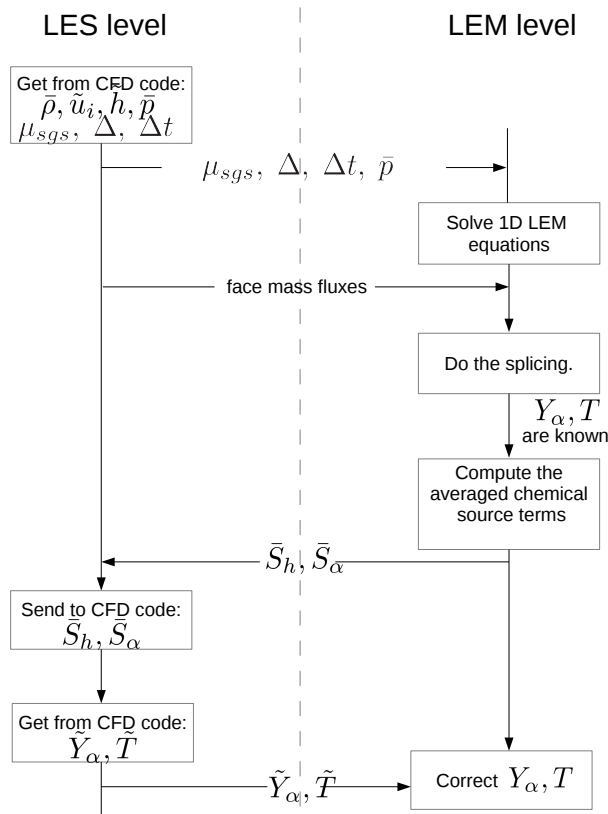


Figure 2. Summary of the steps of the LEM model.

II.F. Numerical method

The conservation equations, Eqs. 1-4, are solved with an adaptation of reactingFoam[®], the reacting solver of the OpenFOAM library. This solver is transient, pressure-based and can handle unstructured meshes.³⁰ A zero-Mach-number assumption is used as done in reactingLMFoam^{31,32} by splitting the pressure into a fluid-mechanical-induced pressure, and a thermodynamic pressure, the latter of which is everywhere constant and it is used to evaluate the equation of state. As a result, acoustic waves are eliminated from the solution. With the present solver, an inner iterative loop is used to correct the velocity field using the output of a pressure equation, as in the well-known PISO algorithm,³³ cf. Tab. 1. Various temporal and spatial discretization options are available from the OpenFOAM library. In the present work, time is discretized with a second-order backward-differencing scheme that uses the current and previous two time-step values. For the convective fluxes, limited linear differencing is used.²⁷ Predictions from the present LESLEM solver are seen to compared well with experiments of a nonreacting mixing problem,³⁰ and with the mean velocity and temperature profiles of a bluff-body-stabilized-flame problem.³⁴

II.G. Configuration

The configuration of present interest is a reacting temporal jet, as depicted in Fig. 3. Initially this flow consists of a fuel slab of thickness H_ξ with its central portion of thickness H having a horizontal velocity of

Table 1. Outline of the algorithm.

Time-advance the LEM equations, Eqs. 10-17, for a LES time interval.
 Calculate the density by solving the continuity equation, Eq. 1.
 Start the outer loop.
 Compute the uncorrected velocity with Eq. 2.
 For LEM conduct the (uncorrected) splicing.
 Compute the mass fractions.
 Compute the sensible enthalpy.
 Compute the temperature from the caloric equation of state, Eq. 6.
 Start the inner loop.
 Get the density from the equation of state, Eq. 5.
 Get the pressure by solving a pressure-correction equation.
 Correct the velocity.
 End of the inner loop.
 For LEM conduct the (corrected) splicing.
 Calculate the turbulence quantities.
 Correct the LEM temperatures and species mass fractions.
 End of the outer loop.

$\Delta U/2$. Its surroundings have velocity of $-\Delta U/2$. The fuel is surrounded by oxidizer. In this way, initially quantities vary only in the vertical direction, y , and are homogeneous in the streamwise, x , and spanwise, z , directions. The vertical profiles of temperature and species mass fraction are given by tangential-hyperbolic functions. The initial temperature and pressure of both the pure fuel and oxidizer streams are T_0 and 101 kPa, and in between the hot products of combustion are given by flamelet solutions. The velocity field consists of a mean spatial profile of horizontal velocity with zero vertical and spanwise components with superimposed fluctuations. The computational domain is a box with dimensions of $L_x \times L_y \times L_z$. A Reynolds number is defined as $\Delta UH/\mu$, and a Damkholer number as $Da = \chi_q H/\Delta U$ with χ_q denoting the scalar dissipation rate at quenching conditions for a flamelet solution.

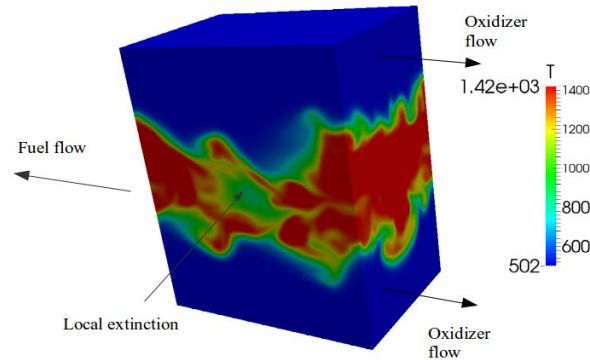


Figure 3. Schematic of the present flow configuration.

Two types of temporal jets are considered here: the syngas, Case-H jet of Hawkes et al.,²⁶ and the ethylene, Case-3 jet of Lignell et al.⁹ The parameters for these flow problems are indicated in Tab. 2. For the syngas simulations the same chemical mechanism as the DNS is used. However, for the ethylene simulations the mechanism of Lu & Law³⁵ is used rather than that used in the DNS because it can be easily put into a CHEMKIN format. Note that the mechanism of the DNS and that of Lu & Law³⁵ are both derived from the same parent mechanism. Two meshes are considered: a coarse mesh with $N_x \times N_y \times N_z = 25 \times 60 \times 17$, and a fine mesh of $108 \times 126 \times 72$. The coarse mesh is nonuniform along y and has more cells near

the initial fuel core, and the fine mesh is uniform and is similar to one use in a previous study.³⁶ Minimum (maximum) mesh spacings are about 0.35 (0.6) mm with the coarse mesh, and 0.13 (0.13) mm with the fine mesh. This coarse mesh has mesh spacings of about three times larger or more than previous studies of the syngas flame.^{36,37} However, it still leads to eddy viscosities of the order of the fuel viscosity at initial conditions. LEM simulations, due to their computational expense, are only conducted with the coarse mesh. Note that in contrast the DNS use mesh spacings of 0.015-0.019 mm. For the boundary conditions, cyclic boundaries are used in the x and z direction, and zero-normal-gradients in the y direction for all quantities except pressure, which is set to one atmosphere at boundaries normal to the y direction. Various parameters for the simulations considered here are indicated in Tab. 3.

Table 2. Parameters used in the syngas and ethylene flame simulations.

Parameter	Syngas flame	Ethylene flame
Fuel	50% CO, 10% H ₂ , 40% N ₂	42.2% C ₂ H ₄ , 57.8% N ₂
Oxidizer	25% O ₂ and 75% N ₂	26.9% O ₂ , 73.1% N ₂
T_0 (K)	500	550
$L_x \times L_y \times L_z$ (mm)	16.4×20×11	11.52×18.24×7.68
H (mm)	1.37	0.96
H_ξ (mm)	1.84	1.5
ΔU (m/s)	138	196
Re	9079	5120
χ_q (1/s)	2380	2380
Da	0.011	0.011
ξ_{st}	0.422	0.17

Table 3. Simulations considered in the present work. Notes: ¹ Model parameters varied as discussed in text.

Flame	Eddy viscosity model	Turbulent combustion model	Mesh
Syngas	Smagorinsky	No-model	Coarse
Syngas	Smagorinsky	No-model	Fine
Syngas	Smagorinsky	LEM ¹	Coarse
Syngas	Smagorinsky	PaSR	Coarse
Syngas	One eq. eddy	No-model	Coarse
Ethylene	Smagorinsky	No-model	Coarse
Ethylene	Smagorinsky	No-model	Fine
Ethylene	Smagorinsky	LEM	Coarse
Ethylene	Smagorinsky	PaSR ¹	Coarse

An important difference between the present LES and the DNS is the setting of the initial velocity fluctuations. The DNS uses broadband turbulent fluctuations with an integral length-scale of about $H/3$. The problem when using these fluctuations is that some information is inevitably lost when using meshes for the LES that are not as fine as those used in the DNS. If such LES meshes are not too coarse, as those used in past LES studies of the syngas flame^{36,37} (and note that in one of these studies the minimum vertical grid spacing is the same as that in the DNS³⁷) this loss of information can be said to be not too detrimental. However, the present goal is to use more practical, coarser meshes than these previous LES, in which case the loss of information from the DNS initial conditions is not negligible anymore. Therefore, following the qualitative nature of the present work, all present LES are initialized with the the $t=0.0002$ s fields (for both syngas and ethylene flames) from a no-model, coarse and Smagorinsky simulation. This simulation in turn is initialized using spatially-averaged (in x and z) DNS data and using zero initial velocity fluctuations.

III. Results

In the following emphasis is made on how temperature maps predicted with LES differ between each other and with DNS data. For this purpose, the next discussion addresses how such differences arise by making a parameter change starting from a base case, which is denoted with bold letters in Tab. 3.

For the syngas simulations, Fig. 4 shows temperature maps in y - t space and ξ - t space from the DNS. Here ξ is the mixture fraction. Both T and ξ have been spatially-averaged along the xz plane. In Fig. 4a the temporal evolution of temperature in the present temporal jet is analogous to that along the streamwise spatial coordinate in a spatially-developing jet. Notice in Fig. 4a that the temperature initially drops and increases later on. This is the process of extinction and reignition. It is interesting to note that the temporal evolution of this process in Fig. 4a looks similar to liftoff in spatially-developing jets.² Figure 4b is useful because it provides in a compact way information about the mixing as well as that of the temperature. Furthermore, the fact that this flame is predominantly non-premixed, as discussed later, allows the use of mixture fraction to present the results. Thus, this type of map is used next when discussing LES results. As in Fig. 4a, the process of extinction and reignition can also be seen in Fig. 4b. During extinction, notice that minimum temperatures of about 1000 K occur along the stoichiometric mixture fraction line, denoted with a grey horizontal line. In addition, the slope of the curve between the color portion of Fig. 4b and the white portion is indicative of the rate of mixing since as the mixing between the fuel and oxidizer happen the maximum value of the mixture fraction decreases. In particular, note that at times larger than $5E-5$ s there is no pure fuel anymore.

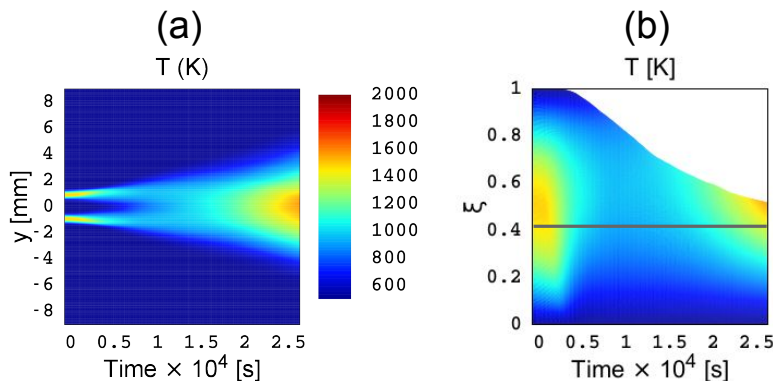


Figure 4. DNS temperature maps for the syngas jet: (a) in y - t space, (b) in ξ - t space.

The comparison between DNS and LES temperature maps is given in Fig. 5. In Fig. 5 as well as in other figures below all LES maps are shifted to visually match the DNS data. This is necessary due to the different initial conditions used. First, notice in Fig. 5 that all LES predict both extinction and reignition. This adequate prediction of the extinction also correlates with the observation that it happens during a time interval where there are high values of the resolved scalar dissipation rate χ , shown as χ/D in Fig. 6 for the base conditions, with D being the diffusivity. Recall that in nonpremixed flames it has been stated that extinction happens when the values of the scalar dissipation rate are high enough for long enough times.³⁸ However, the minimum temperatures predicted with LES during extinction are not as low as those seen in the DNS. Moreover, the extinction-reignition process is slightly faster with LES. Figures 5b and 5c also shows that for the no-model simulations refining the mesh delays the reignition and produces lower temperatures during it, both observations that agree better with the DNS. In regards to the effect of the turbulent combustion model, Figs. 5c and 5d show that the temperature maps with the no-model approach and LEM are almost the same. This observation is also seen when decreasing C_λ from 1 to 0.1 (to produce more triplet maps), when increasing the number of LEM cells per LES cell from 12 to 36, and when turning off the temperature correction explained above. Figures 5c and 5e also show that the effect of using the one-equation-eddy model instead of the Smagorinsky model is small. In contrast with the effect of using LEM or the one-equation-eddy model, Figs. 5c and 5f show that using the PaSR does have an effect on the

predictions, and indeed it appears to make them closer to those using the fine mesh and, as discussed earlier, more accurate in comparison with the DNS.

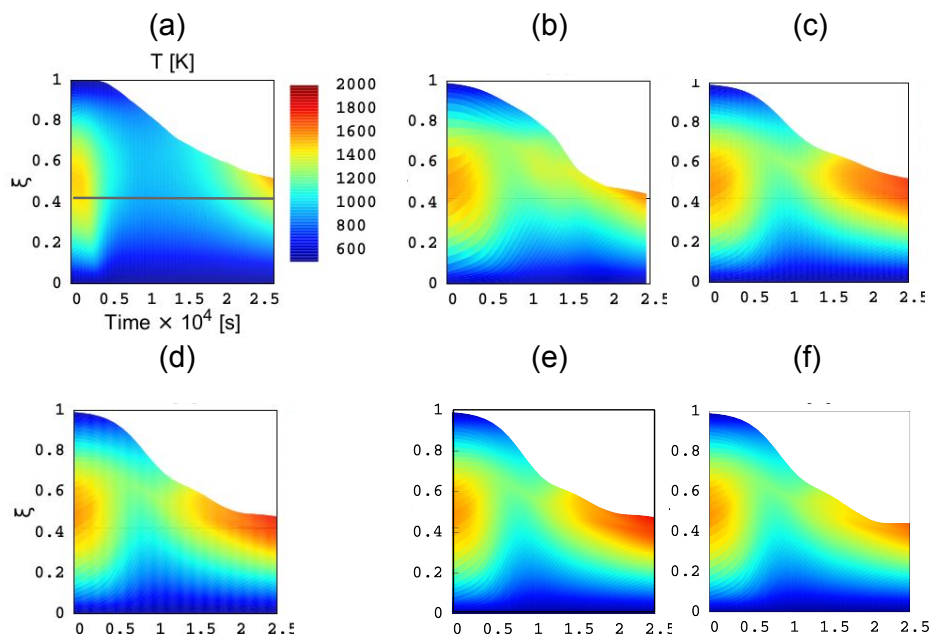


Figure 5. Comparison between DNS and LES temperature maps in ξ - t space for the syngas jet: (a) DNS; (b) no-model, fine mesh, Smagorinsky; (c) no-model, coarse mesh, Smagorinsky; (d) LEM, coarse mesh, Smagorinsky; (e) no-model, coarse mesh, one-equation-eddy model; (f) PaSR, coarse mesh, Smagorinsky.

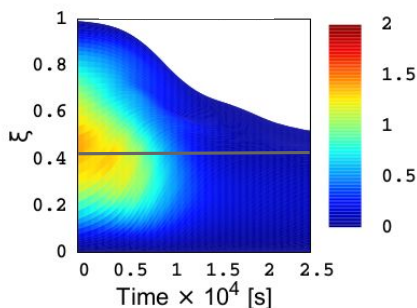


Figure 6. Map of χ/D ($\times 10^{-6} m^{-2}$) in ξ - t space for the base conditions of the syngas jet.

For the ethylene flame, Fig. 7 shows the temperature maps from DNS simulations. Notice that, by comparing the $t=0$ region in Figs. 4b and Fig. 7b, the maximum temperatures are spread over a large interval in mixture fraction space in the syngas flame in comparison with the ethylene flame. (This can be better seen in the heat-release plots in Fig. 17 of Lignell et al.¹⁰). This suggests that the syngas flame is more distributed, whereas the ethylene flame is more flamelet-like. As a result, the process of extinction and reignition is markedly different. Figures 4 and 7 show that the temperature decrease during extinction is larger in the ethylene flame, but the temperature increase during reignition is less. In other words, the extinction is more violent and the reignition is milder in the ethylene flame. In fact, in the ethylene flame, reignition is seen to occur when an isolated flame kernel about 2 mm in diameter reignites the whole flame

after a premixed mixture has been established (Fig. 4 in Lignell et al.⁹). As this happens, the flame changes its character from predominantly nonpremixed to premixed (Fig. 12 in Lignell et al.⁹), as shown later.

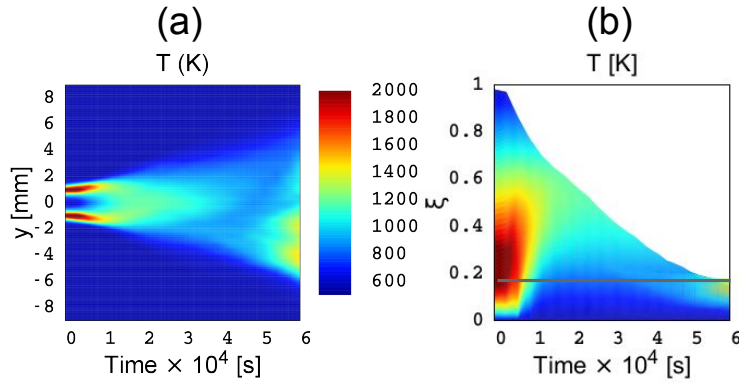


Figure 7. DNS temperature maps for the ethylene jet: (a) in y - t space, (b) in ξ - t space.

Figure 8 shows that, as in the syngas flame, present LES capture the process of extinction and reignition in the ethylene flame. In addition, also as shown in the syngas flame, the extinction happens during a time period of large resolved scalar dissipation rates, as can be seen by comparing Figs. 8 and 9. However, also note in Fig. 8 that the process of extinction and reignition with LES is about two times faster than that seen in the DNS. Moreover, the LES predict larger minimum temperatures during extinction, and the reignition occurs at a higher value of mixture fraction (not shown), at a time where the mixture is less diluted than the DNS. Nonetheless, Figs. 8b and 8c also show a slight enhancement of accuracy by refining the mesh. More interestingly, the use of turbulent combustion models seems to also enhance the accuracy. In particular, the best agreement with the minimum temperatures during extinction is given by the PaSR simulation with the coarse mesh, as can be seen in Fig. 8e. It is also seen that with the PaSR model varying the model constant c_m from 10 to 1 produces negligible differences.

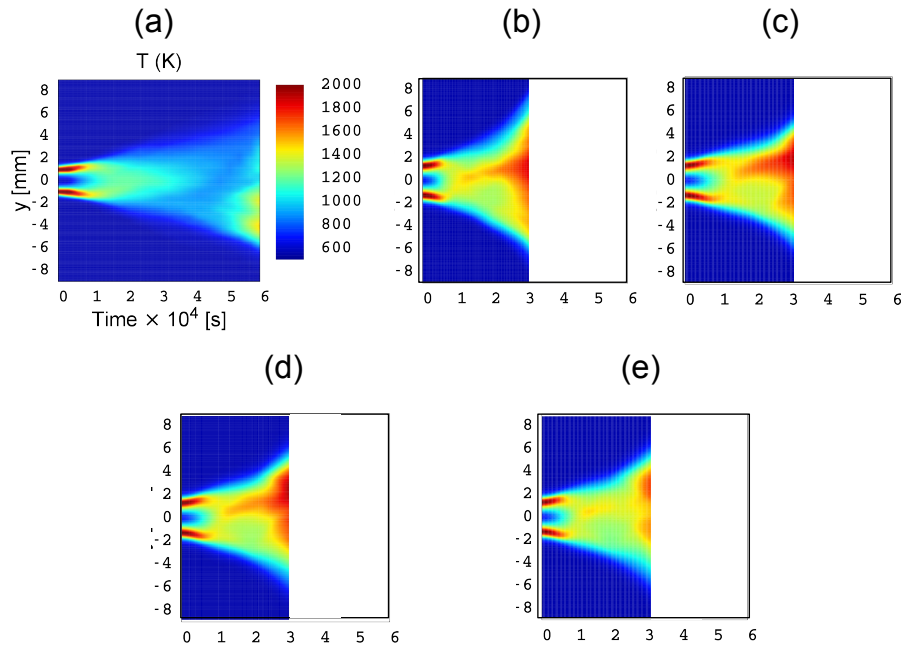


Figure 8. Comparison of temperature maps in y - t space between DNS and LES maps for the ethylene jet: (a) DNS, (b) no-model fine mesh, (c) no-model coarse mesh, (d) LEM coarse mesh, (e) PaSR coarse mesh.

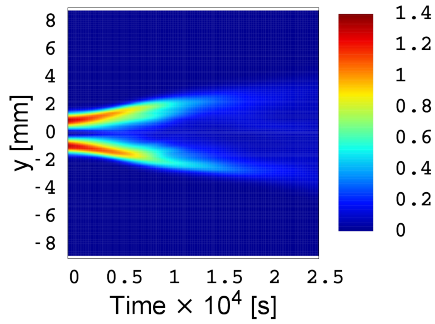


Figure 9. Map of χ/D ($\times 10^{-6} m^{-2}$) in y - t space for the base conditions of the ethylene jet.

Further details about the process of extinction and reignition in the ethylene flame are given in Figs. 10 and 11. Figure 10 shows the temperature field near the point of maximum extinction. Notice in Fig. 10 that the amount of left-over flame after the extinction, represented here by high-temperature regions, is larger with the no-model simulation than with the PaSR simulation. Thus, the latter agrees better with DNS, as discussed above, although the size of the residual flame kernel is larger. Nonetheless, both no-model and PaSR simulation, as well as LEM, do capture the transition from nonpremixed flame to premixed flame seen in the DNS (Fig. 12 in Lignell et al.⁹). This can be seen in Fig. 11, where the premixed line represents the integration of the PDF of flame index weighted by the heat-release rate having values greater than 0.707, while the nonpremixed line does the same for values less than -0.707. Here the flame index is defined as the normalized product of the gradient of fuel concentration and gradient of oxidizer concentration. All quantities used for these calculations are filtered quantities. In contrast with the ethylene flame, as can be seen in Fig. 12, it is interesting to notice that the flame is predominantly non-premixed in the syngas case.

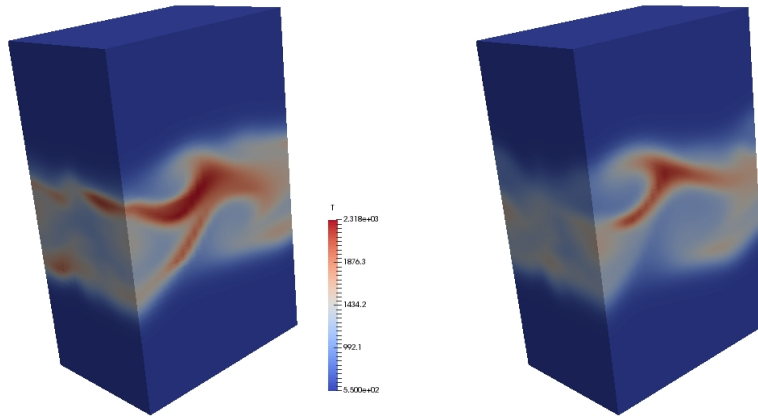


Figure 10. Temperature field near the time of maximum extinction with the no-model approach (left) and with the PaSR model (right). Other parameters include coarse mesh and Smagorinsky.

IV. Analysis

Overall the present LES capture the process of extinction and reignition in two types of jets. For the ethylene flame, this result is an enhancement of accuracy over a previous study using the one-dimensional turbulence model which does not capture reignition.¹⁰ Furthermore, the change from non-premixed to premixed combustion in this flame is captured.

The accuracy of the present predictions, nonetheless, can not be deemed fully satisfactory. In fact,

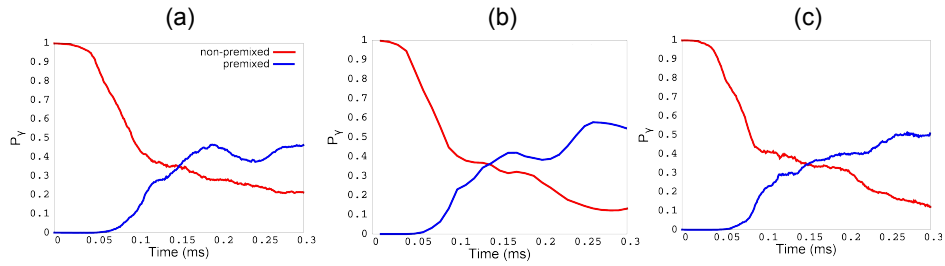


Figure 11. Temporal evolution of the nonpremixed or premixed character of the ethylene flame as explained in the text: (a) no-model, (b) LEM, and (c) PaSR.

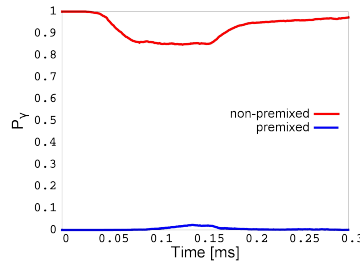


Figure 12. Temporal evolution of the nonpremixed or premixed character of the syngas flame as explained in the text with the no-model approach, coarse mesh, and Smagorinsky model.

for the syngas flame, such an accuracy is inferior to that from previous studies with the transported-PDF method³⁶ and the LEM model.³⁷ However, these two studies used very fine meshes (in fact, the latter one uses a minimum vertical grid spacing similar to the DNS), and the present focus is on coarse meshes of more practical relevance, as well as on exposing model deficiencies with this type of meshes. In spite of this low accuracy, the present work has some value in showing how predictions are sensitive to model variations.

In both flames a sensitivity to variations of the turbulence modeling has been observed. Furthermore, refining the mesh improves the accuracy of the predictions. Thus, it is unlikely that most of the relevant scales are being well resolved. Such a sensitivity appears to be more pronounced in the ethylene flame during the reignition stage when the flame transitions from predominantly nonpremixed to premixed. In this case, no-model (laminar chemistry) predictions with the coarse mesh are made more accurate by using the LEM model and, more notably, with the use of the PaSR model. For the latter model, this is seen both in temperature maps and the detailed evolution of the flowfield. Thus, it cannot be said that in general there is no need for turbulence modeling for problems such as the present ones.

Such an apparent enhancement of accuracy with turbulence modeling can be partly explained as follows. DNS observations show that the effect of the unsteady scalar dissipation rate has a profound effect on the extinction happening early on.¹⁰ The full resolution of these physics is not possible with the present coarse-mesh LES. In this case, in the PaSR model the effect of the scalar-dissipation fluctuations on the flame are empirically modeled through the effect of the subgrid eddy viscosity on the mixing time scale of the PaSR model, τ_m , cf. Eq. 8. With LEM this effect is modeled by the action of the triplet maps on the subgrid 1D profiles, a process that also depends on the subgrid eddy viscosity. In addition, the eddy viscosity affects the transport of cold ambient fluid into the reacting core. This is how the turbulent-combustion model and the eddy-viscosity model act to represent physics not resolved by the mesh.

Lastly, it must be noted that an important question has been left unanswered: Is the apparent enhancement of accuracy produced by the turbulence modeling a result of better representing the unresolved physics or of having a dynamical system (the flame) which is very close to a bifurcation (stable-burning to blowoff) and thus very sensitive to model-parameter variations? To address this question, a more in-depth analysis than the present one using mean temperature maps is needed using, for example, plots of various quantities

versus instantaneous values of the resolved and modeled scalar dissipation rates.

V. Conclusions

1. Present LES with a rather coarse mesh capture qualitatively the extinction and reignition observed in DNS simulations of two types of reacting jets.
2. The sensitivity to the turbulent-combustion model is not negligible, and the best accuracy is seen with the PaSR model.
3. The number of models and model-parameter space considered in this work are small and should be augmented to provide best-practice recommendations on how to model extinction and reignition.
4. Overall, the accuracy of the present LES when compared with the DNS is not satisfactory. If this result is not mainly due to the different initial conditions used, then the problem of how to accurately model extinction and reignition with practically-relevant meshes remains open.
5. The issue of how accurate model predictions need to be for practical applications also remains open. For instance, is the expectation for the models to closely match the time-history of the DNS fields? Or should models be assessed in a probabilistic manner (e.g. by addressing what is the probability of extinction in an ensemble of simulations)?

Acknowledgments

The authors will like to thank Evatt Hawkes for providing the syngas DNS data and Alan Kerstein and Suresh Menon for helpful discussions. This work was conducted thanks to the financial support from the Small-Business-Innovation-Research / Small-Business-Technology-Transfer project titled ‘Physical submodel development for turbulence combustion closure’, contract number FA9550-15-C-0044.

Appendix: Further details about the splicing algorithm

The transfer of LEM elements (mass) between different LES cells is done with a Lagrangian-based, mass-transfer algorithm called splicing. This algorithm has two main steps.

In the first step, the amount of mass to be transferred through the face of two adjacent LES cells is computed. It is useful to consider a donor LES cell (one that donates mass) and a receiver LES cell (one that receives mass), a denomination which is dictated by the sign of the mass flux, as explained shortly. The mass in the LEM domains to be transferred between adjacent LES cells, and related mass flux, has a contribution due the the resolved velocity, M_{res} , and one from the subgrid-scale velocity, M_{sgs} . They are respectively given by

$$M_{res} = m\Delta t A \tilde{u} V^{-1}, \quad (19)$$

$$M_{sgs} = m\Delta t A u_{sgs} V^{-1}. \quad (20)$$

Here m is the total mass in the LEM domain of a given LES cell, Δt is the LES time step, A is the area of the common face between donor and receiver LES cells, \tilde{u} is the velocity normal to the face, u_{sgs} is an estimate of the subgrid-scale velocity at the face (computed from the LES model), and V is the volume of the donor LES cell. The sign of $M_{res} + M_{sgs}$ dictates whether a LES cell is donating or receiving mass. At this point, for a given LES cell and its respective LEM domain, we know the amount of mass $M_{res} + M_{sgs}$ that needs to be cut (removed away) from the LEM domain into each of the adjacent LES cells, cf. Fig. 13. But in which order?

The second step of the splicing is to decide in which order to cut and paste LEM elements, cf. Figs. 14. The need of such decision is a consequence of having two ends of the LEM domain and six or more faces in a LES cell. The following rules are followed in this decision. First, the outflow is done from one end of the LEM domain, and the inflow through the other end. Thus, the segments to be spliced are considered as flowing along the LEM domain (meaning starting from the domain state prior to modification by splicing) and being ejected from the domain through the output boundary, and thus available for transfer across an LES face. Second, the segments associated with the lowest flux $M_{res} + M_{sgs}$ are removed first, and those

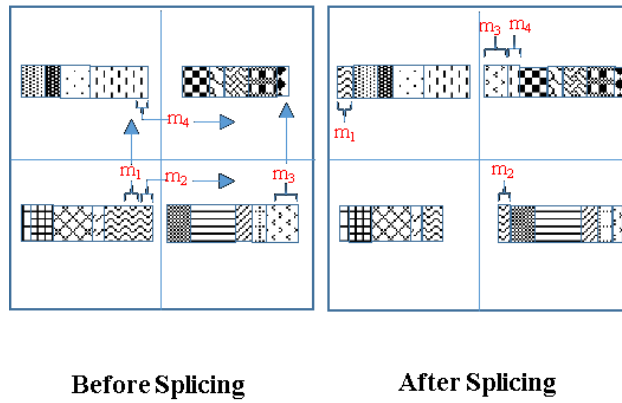


Figure 13. Splicing algorithm.

associated with the highest flux are removed last, cf. Fig. 14a. Third, in a similar manner, the segments associated with the highest flux are pasted (attached) first to the inflow side of the LEM, and those with the lowest flux are pasted last, cf. Fig. 14b. This second and third rules are consistent with the idea that the low-flux segments have less momentum than the high-flux segments, so the former are displaced less along LEM lines, cf. Fig. 14c.

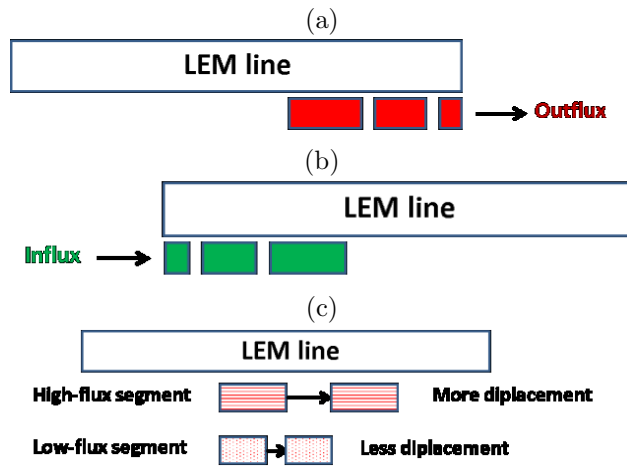


Figure 14. Step 2 of the splicing algorithm.

Further implementation details are as follow. The splicing algorithm is implemented by looping three times over all LES cells in the whole computational domain. During the first loop, following step 1, the magnitude and direction of mass flux on each LES cell face are calculated. An empty list is attached to each LES face. In the second loop, following step 2, all outflux faces of an LES cell are identified and their respective outflux masses are gathered and sorted in ascending order. Then the outflux LEM segments corresponding to the outflux masses are spliced (cut and pasted) in ascending order of outflux mass from the splicing donor LEM line to the corresponding empty lists (attached to each LES face). This procedure is repeated for all other LES cells until the second loop is finished and all empty lists are now filled. Using the same principle, in the third loop, all the influx faces of a LES cell are recognized and their respective influx masses are sorted in descending order. Then the LEM segments are spliced in descending order (of influx mass) to the splicing receiver LEM line from the corresponding filled lists (attached to each LES face). The third loop goes through all LES cells and in the end all the filled lists resulting from the first loop are empty again. The splicing process is complete.

The standard splicing algorithm on a single processor domain has been implemented very efficiently using a pointer based LEM data structure where splicing is realized via simple pointer re-arrangements. However,

domain decomposition for parallel computations on distributed memory architectures leads to processor domains which have a priori no input from neighboring processor domains. If splicing is not done correctly (e.g. by a simplified cell averaged approach) at processor boundaries, it can lead to unphysical results. In order to perform splicing across processor boundaries, LEM lines across processor boundaries (called ghost LEM lines) are copied to the neighboring processor. Then splicing is performed between LEM lines that are next to the boundary and ghost LEM lines by each processor.

References

- ¹Turns, S. R., *An introduction to combustion*, McGraw-Hill, 1996.
- ²Peters, N., *Turbulent combustion*, Cambridge University Press, 2000.
- ³Fox, R. O., *Computational models for turbulent reacting flows*, Cambridge University Press, 2003.
- ⁴Poinsot, T. and Veynante, D., *Theoretical and numerical combustion*, RT Edwards, Inc., 2005.
- ⁵Cant, R. S. and Mastorakos, E., *An introduction to turbulent reacting flows*, World Scientific, 2008.
- ⁶Shanbhogue, S. J., Husain, S., and Lieuwen, T., “Lean blowoff of bluff body stabilized flames: Scaling and dynamics,” *Progress in Energy and Combustion Science*, Vol. 35, No. 1, 2009, pp. 98–120.
- ⁷Hewson, J. and Kerstein, A., “Stochastic simulation of transport and chemical kinetics in turbulent CO/H₂/N₂ flames,” *Combustion Theory and Modelling*, Vol. 5, No. 4, 2001, pp. 669–697.
- ⁸Fru, G., Janiga, G., and Thévenin, D., “Direct Numerical Simulations of the Impact of High Turbulence Intensities and Volume Viscosity on Premixed Methane Flames,” *Journal of Combustion*, 2011.
- ⁹Lignell, D., Chen, J., and Schmutz, H., “Effects of Damköhler number on flame extinction and reignition in turbulent non-premixed flames using DNS,” *Combustion and Flame*, Vol. 158, No. 5, 2011, pp. 949–963.
- ¹⁰Lignell, D. O. and Rappleye, D. S., “One-dimensional-turbulence simulation of flame extinction and reignition in planar ethylene jet flames,” *Combustion and Flame*, Vol. 159, No. 9, 2012, pp. 2930–2943.
- ¹¹Knudsen, E. and Pitsch, H., “Large-Eddy Simulation for Combustion Systems: Modeling Approaches for Partially Premixed Flows,” *Open Thermodynamics Journal*, Vol. 4, 2010, pp. 76–85.
- ¹²Haworth, D. C., “Progress in probability density function methods for turbulent reacting flows,” *Progress in Energy and Combustion Science*, Vol. 36, No. 2, 2010, pp. 168–259.
- ¹³Barlow, R. S. and Frank, J. H., “Effects of turbulence on species mass fractions in methane/air jet flames,” *Proceedings of the Combustion Institute*, Vol. 27, No. 1, 1998, pp. 1087–1095.
- ¹⁴Barlow, R. S., Meares, S., Magnotti, G., Cutcher, H., and Masri, A. R., “Local extinction and near-field structure in piloted turbulent CH₄/air jet flames with inhomogeneous inlets,” *Combustion and Flame*, Vol. 162, No. 10, 2015, pp. 3516–3540.
- ¹⁵Pope, S. B., “Small scales, many species and the manifold challenges of turbulent combustion,” *Proceedings of the Combustion Institute*, Vol. 34, No. 1, 2013, pp. 1–31.
- ¹⁶Sankaran, V. and Merkle, C. L., “Fundamental Physics and Model Assumptions in Turbulent Combustion Models for Aerospace Propulsion,” *AIAA Paper 2014-3941*, 2014.
- ¹⁷Gonzalez-Juez, E. D., Kerstein, A. R., Menon, S., and Ranjan, R., “An analysis of the basic assumptions of turbulent-combustion models with emphasis on high-speed flows,” *AIAA Paper 2015-1380*, 2015.
- ¹⁸Oefelein, J. C., “Analysis of turbulent combustion modeling approaches for aero-propulsion applications,” *AIAA Paper 2015-1378*, 2015.
- ¹⁹Miller, R. S. and Foster, J. W., “Survey of Turbulent Combustion Models for Large-Eddy Simulations of Propulsive Flowfields,” *AIAA Journal*, 2016, pp. 1–17.
- ²⁰Kerstein, A. R., “A linear-eddy model of turbulent scalar transport and mixing,” *Combustion Science and Technology*, Vol. 60, No. 4-6, 1988, pp. 391–421.
- ²¹Kerstein, A. R., “Linear-eddy modelling of turbulent transport. Part 7. Finite-rate chemistry and multi-stream mixing,” *Journal of Fluid Mechanics*, Vol. 240, 1992, pp. 289–313.
- ²²Menon, S., Kerstein, A. R., and McMurtry, P. A., “A linear eddy mixing model for large eddy simulation of turbulent combustion,” *Large Eddy Simulation of Complex Engineering and Geophysical Flows*, 1993, pp. 287–314.
- ²³Menon, S. and Kerstein, A. R., “The Linear-Eddy Model,” *Turbulent Combustion Modeling*, 2011, pp. 221–247.
- ²⁴Nordin, P. A., *Complex chemistry modeling of diesel spray combustion*, Ph.D. thesis, Chalmers University of Technology, 2001.
- ²⁵Magnussen, B. F., “The Eddy Dissipation Concept—A Bridge Between Science and Technology,” *ECCOMAS thematic conference on computational combustion*, 2005, pp. 21–24.
- ²⁶Hawkes, E. R., Sankaran, R., Sutherland, J. C., and Chen, J. H., “Scalar mixing in direct numerical simulations of temporally evolving plane jet flames with skeletal CO/H₂ kinetics,” *Proceedings of the combustion institute*, Vol. 31, No. 1, 2007, pp. 1633–1640.
- ²⁷OpenFOAM, <http://www.openfoam.org/>.
- ²⁸Weller, H. G., Tabor, G., Jasak, H., and Fureby, C., “A tensorial approach to computational continuum mechanics using object-oriented techniques,” *Computers in physics*, Vol. 12, No. 6, 1998, pp. 620–631.
- ²⁹Kerstein, A. R., “One-dimensional turbulence: model formulation and application to homogeneous turbulence, shear flows, and buoyant stratified flows,” *Journal of Fluid Mechanics*, Vol. 392, 1999, pp. 277–334.
- ³⁰Arshad, S., Kong, B., Kerstein, A., and Oevermann, M., “A strategy for large scale advection in CFD models using LEM as a LES subgrid mixing model,” *Proceedings of the 4th International Conference on Computational Heat and Mass Transfer*, 2016.

³¹Duwig, C., Nogenmyr, K., Chan, C., and Dunn, M. J., “Large Eddy Simulations of a piloted lean premix jet flame using finite-rate chemistry,” *Combustion Theory and Modelling*, Vol. 15, No. 4, 2011, pp. 537–568.

³²Fiorina, B., Mercier, R., Kuenne, G., Ketelheun, A., Avdić, A., Janicka, J., Geyer, D., Dreizler, A., Alenius, E., Duwig, C., et al., “Challenging modeling strategies for LES of non-adiabatic turbulent stratified combustion,” *Combustion and Flame*, Vol. 162, No. 11, 2015, pp. 4264–4282.

³³Issa, R. I., “Solution of the implicitly discretised fluid flow equations by operator-splitting,” *Journal of Computational physics*, Vol. 62, No. 1, 1986, pp. 40–65.

³⁴Gonzalez-Juez, E. D., Arshad, S., Oevermann, M., Dasgupta, A., and Menon, S., “Turbulent-combustion closure for the chemical source terms using the linear-eddy model,” *To be presented at the AIAA/ASME/SAE Joint Propulsion Conference.*, 2017.

³⁵Lu, T. and Law, C. K., “A directed relation graph method for mechanism reduction,” *Proceedings of the Combustion Institute*, Vol. 30, No. 1, 2005, pp. 1333–1341.

³⁶Yang, Y., Wang, H., Pope, S. B., and Chen, J. H., “Large-eddy simulation/probability density function modeling of a non-premixed CO/H₂ temporally evolving jet flame,” *Proceedings of the Combustion Institute*, Vol. 34, No. 1, 2013, pp. 1241–1249.

³⁷Sen, B. A. and Menon, S., “Artificial neural networks based chemistry-mixing subgrid model for LES,” *AIAA Paper 2009-241*, 2009.

³⁸Hewson, J. C., “An extinction criterion for nonpremixed flames subject to brief periods of high dissipation rates,” *Combustion and Flame*, Vol. 160, No. 5, 2013, pp. 887–897.